Mine Water and the Environment (2021) 40:209–224
https://doi.org/10.1007/s10230-021-00751-9

TECHNICAL ARTICLE

The Failure of the Aznalcóllar Tailings Dam in SW Spain

Eduardo E. Alonso[1]

Received: 12 March 2020 / Accepted: 14 January 2021 / Published online: 27 January 2021

Abstract
The Aznalcóllar dyke failed and released much of its stored, saturated pyritic tailings after a process of progressive failure in the foundation clay. 1.5 Mm^3 of tailings and 5.5 Mm^3 of acidic water were rapidly discharged from the pond. The paper reviews the main geotechnical aspects that contributed to the development of a sliding surface under the dyke: its downward construction procedure, the brittle nature of the over-consolidated, high plasticity foundation clay, and the prevalent high pore pressures in the clay. The downward construction method created a "wave" of high stress ratios under the advancing toe of the dyke capable of taking the strength from peak to residual values. The brittleness of the foundation clay is very significant because of its high plasticity and the presence of montmorillonite among its mineralogical constituents. The high pore pressures are a consequence of the high density tailings (3.1 g/cc), the low permeability of the clay, and the consolidation process in a dominant upward direction. Also discussed in the paper are the dynamics of the dam failure (displacement, velocity, and acceleration). The geometry of the dyke, in plan view, and its relationship with the direction and dip of the clay layers explains the position of the failure. This paper summarizes the lessons derived from this case history.

Keywords Clay strength · Plasticity · Progressive failure · Landslide · Pore pressure · Liquefaction

Introduction

The Aznalcóllar tailings dam was part of an open pit mining complex that produced copper, zinc, and lead. The major component of the tailings was pyrite (78–83%), along with sphalerite, galena, and chalcopyrite, while non-exploitable rock (shales, greywackes, dacites, and rhyolites) comprised 85% of the total mined volume.

The Aznalcóllar dam was a retention structure for a deposit of saturated pyritic tailings. The dam was a strong rockfill retaining structure built by a downward technique, illustrated in Fig. 1. The figure shows an upstream impervious clay layer, to restrict the water flow, an inner filter, and the rockfill. At the time of failure, the dam was 28 m high and the upper level of the tailings was 2 m below the dam crest. The length of the perimeter dam was 4.5 km. A 600 m long stretch on the southeast side of the dam slid forward, about 50 m, on the 25th of April, 1998. This displacement led to the release of seven million m^3 of liquefied tailings and acid water, which travelled along the valleys of the Agrio and Guadiamar rivers for a maximum distance of 70 km. Figure 2 is a map of the affected area. Fortunately, there were no casualties as a result of water and tailings flow downstream of the dam. The flow stopped right at the edge of the Doñana National Park and the damage was concentrated in a band of toxic tailings filling the valley of the two rivers mentioned. However, this failure triggered a social alarm in the country, in part motivated by the serious threat on the Doñana National Park, an emblematic protected area.

Figure 3 is an aerial picture of the breach opened on the east side of the dam after the main flooding event. The tailings deposit was divided into two ponds (north and south) separated by a transversal dyke shown in the photograph. The southern pond (left part of the photo) stored the finest tailings (fine sand and silt sizes) whereas the northern one received coarser material (medium to fine sands). The deposition of tailings in the pond used a spigotting technique. The deposit remained always saturated under a shallow (≈1 m) water layer. The failure affected the southern deposit.

This paper analyses the reasons for the failure. Previous publications by the author and co-workers, listed in the reference section, include additional information on the failure and its consequences, geometrical and geological details,

✉ Eduardo E. Alonso
eduardo.alonso@upc.edu

[1] Department of Civil and Environmental Engineering, UPC, Barcelona, Spain

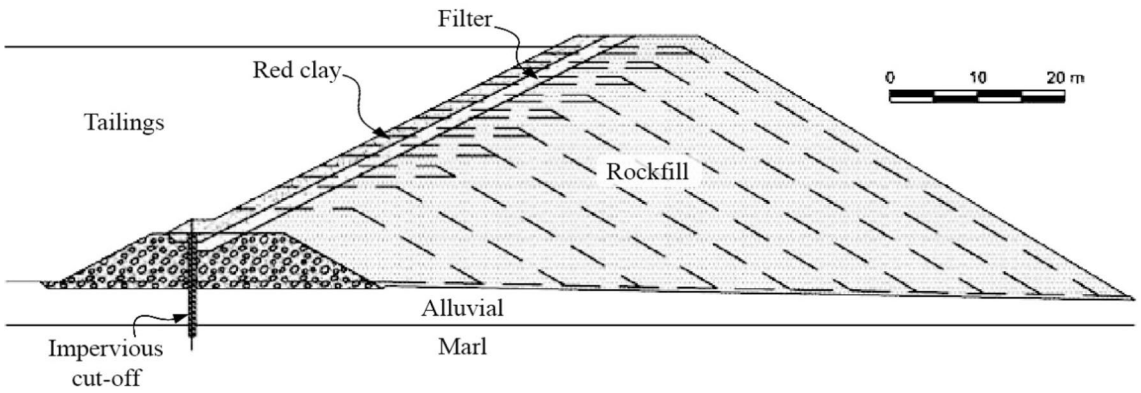

Fig. 1 The original design of the dyke cross section and the specified construction sequence

Fig. 2 Map of affected area (Eriksson and Adamek 2000)

testing procedures, analytical derivations, and computational work. The emphasis here was to isolate the fundamental mechanisms explaining the instability, and its relationship to the adopted construction procedure. Information not essential for these purposes has been omitted. Besides describing the materials involved and the field evidence, the analysis relies on the modelling of significant aspects and its comparison with observations. In addition, the lessons

Fig. 3 April 25, 1998; early morning. On the left, the displaced stretch of the dam and the opening allowed a fraction of the stored tailings and water to spill out, north and south of the transversal dyke. The original breach was estimated at about 14 m wide. Subsequent erosion increased the gap to about 25 m

offered are summarized with reference to provisions of the original design and the accumulated experience from other known cases related to the Aznalcóllar failure, mainly regarding the topic of progressive failure of dams, embankments, and slopes (Cooper et al. 1998; Potts et al. 1990; Stark and Eid 1994; Yerro et al. 2016).

Field Observations and Material Properties

Figure 4 is an illustrative cross section of the southern pond, the one involved in the failure (Alonso and Gens 2006a). The waste was confined by a perimeter dyke, which had its maximum height on the eastern side. On the opposite western side, a natural hill helped to complete the tailings enclosure. The dyke and the waste rested on an alluvial permeable terrace, 3–4 m thick, which overlaid a 60–70 m thick deposit of over-consolidated brittle marine clays of Pliocene age. A thin aquifer covering a Paleozoic substratum provided the lower boundary for the Tertiary clay, known locally as the Guadalquivir blue clay.

The blue clay layers dip 2°–4° towards the SSE. There are some indications of striations of the planar stratification layers. Vertical jointing was also measured in exposures, dominantly oriented in the NE–SW direction.

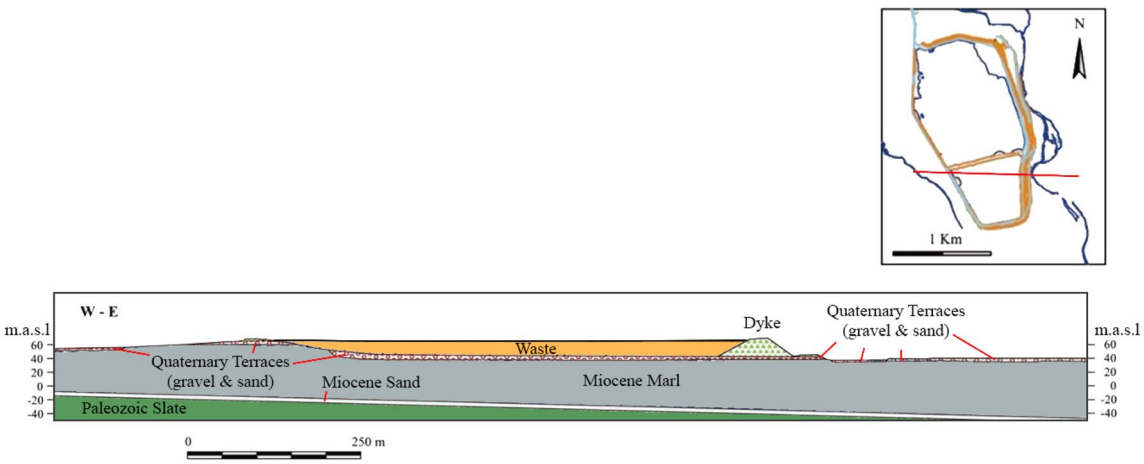

Fig. 4 Representative geological profile

Aerial photographs taken before and after the accident provided a precise description of the failure. A 600 m long stretch of the southern dyke moved to the east (Fig. 5). The displacement vectors represented in Fig. 5 reached maximum values of 45–55 m in the central part of the displaced dyke. Towards the north and south, the displacements decreased gradually. The breach occurred at a place where the dyke's orientation changed. In fact, the dyke limiting the northern pond of the deposit remained essentially still, as explained below. In some locations, the horizontal (D_h) and vertical (D_v) displacements of the displaced points could be determined. The spatial direction of the displacement vectors at these points followed the dip direction of the stratification planes. The vertical jointing of the clay substratum explains some aspects of the slide geometry. The northern limit was a plane separating the stable dyke from the displaced one. The forward sliding motion opened a "window", which allowed the tailings to spill. The dominant family of vertical joints in the NE–SW direction explains the direction of the separating plane. The upstream limit of the landslide was a sub-vertical plane, which is consistent with the vertical dip of the clay joints. Alonso and Gens (2006a) provide additional details on the role of the clay's vertical jointing.

Figure 5 shows the contour of the landslide responsible for the displacement of the dyke. Figure 6 shows the central cross-section of the landslide after failure. The geometry of the failure surfaces were established by the numerous borings shown in the figure; clear indication of shearing bands were found in the cores. Trenches excavated in the downstream passive zone also helped detail the shearing of the mobilized clay mass.

The violent flow of liquefied tailings out of the pond carried with it large blocks of marine clay, which "floated" on the underlying tailings (Fig. 7), due to the high specific

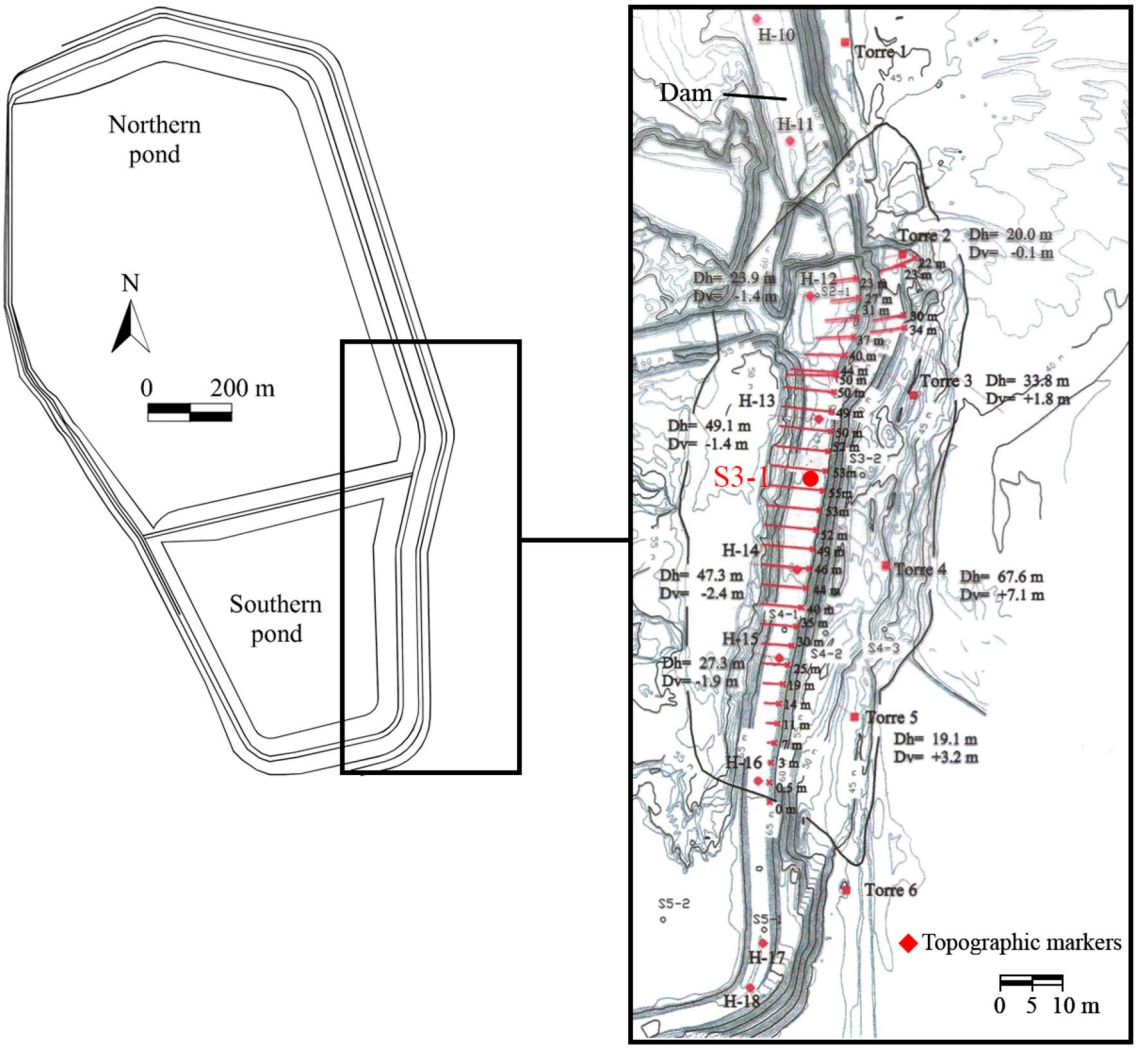

Fig. 5 Landslide contour line and displacement vectors of the southeastern dyke

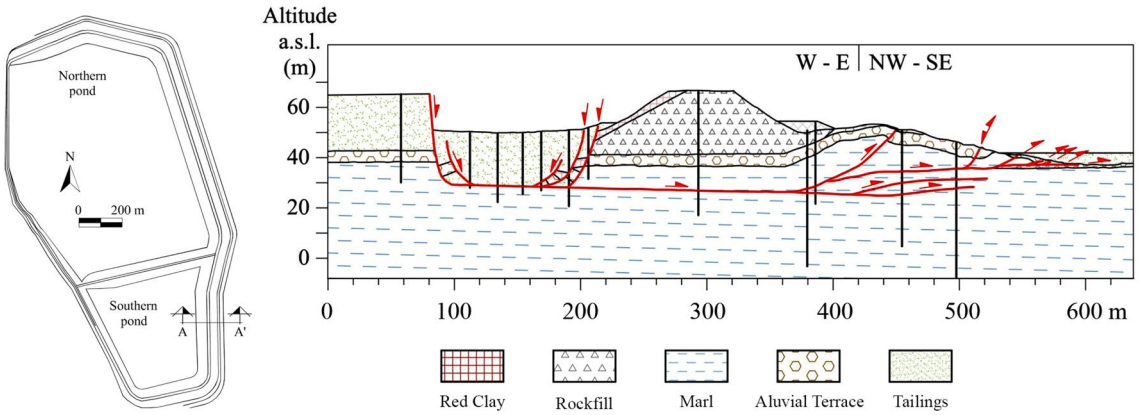

Fig. 6 The central zone of the failure, showing the displaced dam and the pattern of shearing surfaces within the blue clay

Fig. 7 Clay blocks 'floating' on the tailings flow. Note the parallelepipedic shape, sharp edges, and the joints covered by oxidation coatings

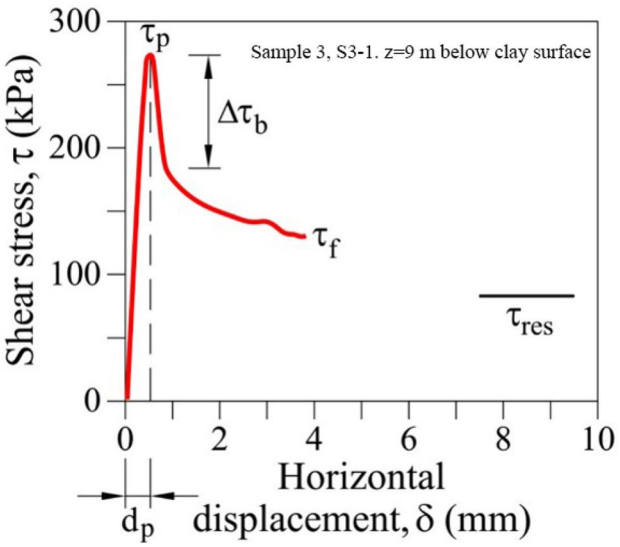

Fig. 8 A drained direct shear test of a 50 mm diameter sample of blue clay under a normal effective stress of 400 kPa. Figure 5 shows the position of boring S3-1

weight of the saturated pyritic tailings (around 31 kN/m^3) and the natural saturated specific weight of the blue clay (18–20 kN/m^3). These blocks exhibited a parallelepipedal geometry, consistent with the set of main discontinuities: sub horizontal sedimentary planes and two families of vertical jointing. These large bodies of blue clay allowed us to extract undisturbed block samples for laboratory testing; Alonso and Gens 2006a).

The following basic data identifies the over-consolidated blue clay:

- Plasticity: $w_L = 67–67\%$; PI = 32–35%
- Fines content > 98%; clay fraction (< 2 μm): 47–58%
- Natural water content: w = 30–35%
- Void ratio: e = 0.8–1.0
- Classification: CH or MH
- Coefficient of consolidation: $c_v = 0.5$ to 1.5×10^{-3} cm^2/s
- Permeability: k = 2 to 7×10^{-9} cm/s
- Clay minerals: calcite + quartz: 30%; calcic smectite: 35%; illite + kaolinite: 35%

The clay deposit is very homogeneous, a condition accepted in all stability calculations. Drained direct shear tests provided good information on the clay's brittleness. Figure 8 shows the shear stress-displacement record for a sample recovered at a depth of 9 m below the upper clay surface.

The set of shear tests performed were also used to determine the shear strength envelopes (Fig. 9). An effective cohesion of 64 kPa and a drained friction angle of 24.1° characterizes peak conditions for very small relative shear displacements (< 1 mm). Further deformation leads to a progressive softening. The residual friction for relative shear displacements in excess of 10 mm was 11°.

From a geotechnical perspective, the stored tailings were silt-sized granular soils. Because of the dominant

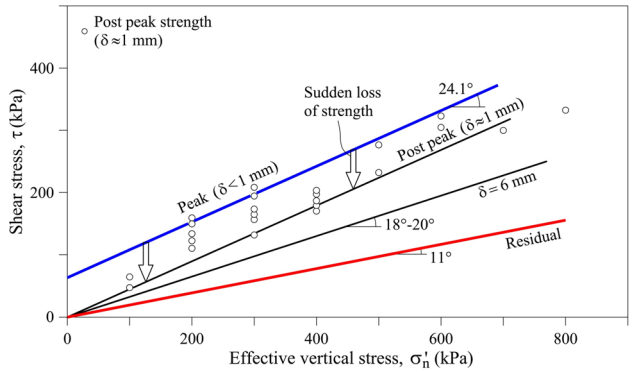

Fig. 9 Strength envelopes of Guadalquivir blue clay based on direct shear tests

proportion of pyritic mineral (density ≈ 4.1 g/cm^3), the bulk total density of the pyritic tailings averaged 3.1 g/cm^3. A series of K_0 undrained triaxial tests indicated an initial tendency for compression ("negative" dilatancy) under shear, which evolved to a marked dilatancy near the failure envelope, characterized by a high friction angle (37°). Measured "in situ" void ratios ranged from 0.6 to 0.8. The water content of the saturated tailings, before the failure, ranged between 15 and 20%. The tailings had a low saturated permeability (10^{-6}–10^{-7} cm/s) and exhibited significant cementation, attributed to the chemicals added during mineral processing and the long deposition period (the tailing's deposition started in 1976, 22 years before the failure). Indications of cementation were the measured unconfined compression strength of undisturbed samples (100–200 kPa) and the effective cohesion identified in shearing tests (c'≈17 kPa).

Modelling Progressive Failure

A key aspect of the failure was the pore pressure measurements in the foundation blue clay in locations not directly affected by the landslide. The northern dyke, which did not fail, was a convenient choice to install a few vibrating wire piezometers because its geometry and construction history was identical to conditions of the failed southern dyke. Figure 10 shows some measurements taken more than a year after the failure. Despite the time elapsed without any further raising of the dam and the partial unloading of the tailings weight, the pore pressures a few meters below the upper clay boundary were still very high, due to the low, homogeneous clay permeability. This information was the starting point for a simplified analytical procedure to determine the evolution of stresses and pore pressures on the foundation clay during the entire construction history of the deposit. Alonso and Gens (2006a) and Gens and Alonso (2006) provide details of this analysis, which relied on the following assumptions:

- Total foundation stresses follow analytical solutions for an elastic half space and the principle of superposition;
- The instantaneous increase in pore pressure, induced by an increment of external loading (increase in tailings level and dam heightening) is equal to the increment of mean total stress;
- Pore pressures dissipate according to the solution for the consolidation equation for a semi-infinite medium. These pressures accumulate and dissipate following the history of dam construction.

This procedure provided a good indication of the process of progressive failure experienced by the foundation clay during the forward construction of the dike. Figure 11 shows the actual sequence of dam construction.

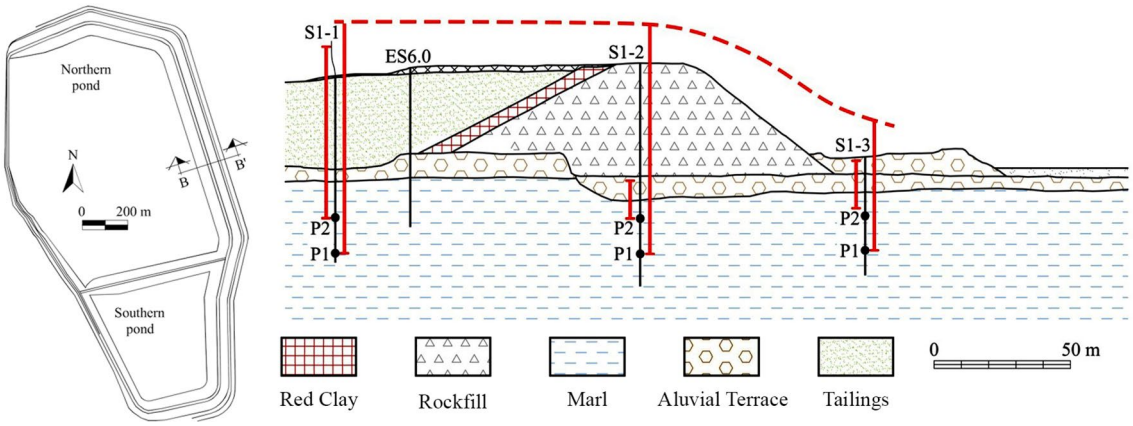

Fig. 10 Measured pore water pressure profile in northern dyke after failure of the southern dyke, October 1999. (The length of the red segments, at the scale of the figure, provides the piezometric head at the considered point)

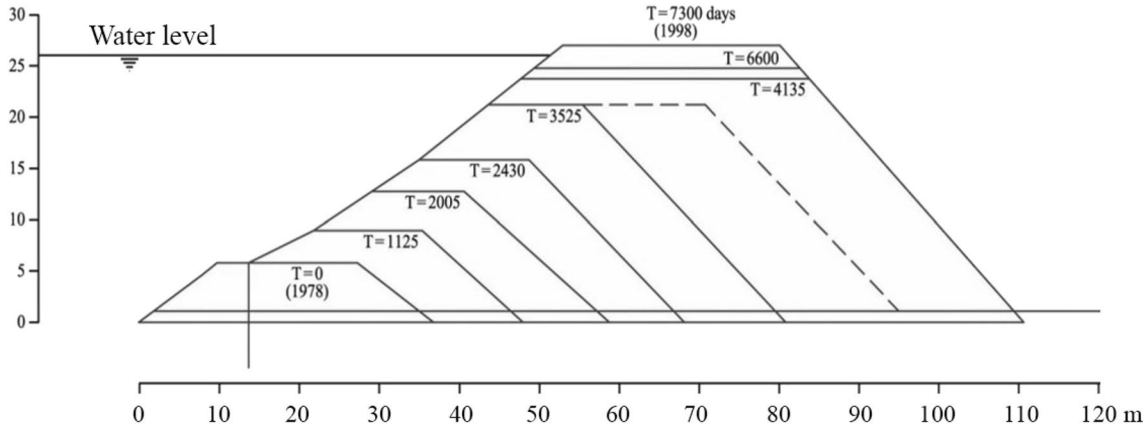

Fig. 11 The evolving geometry of Aznalcóllar dam

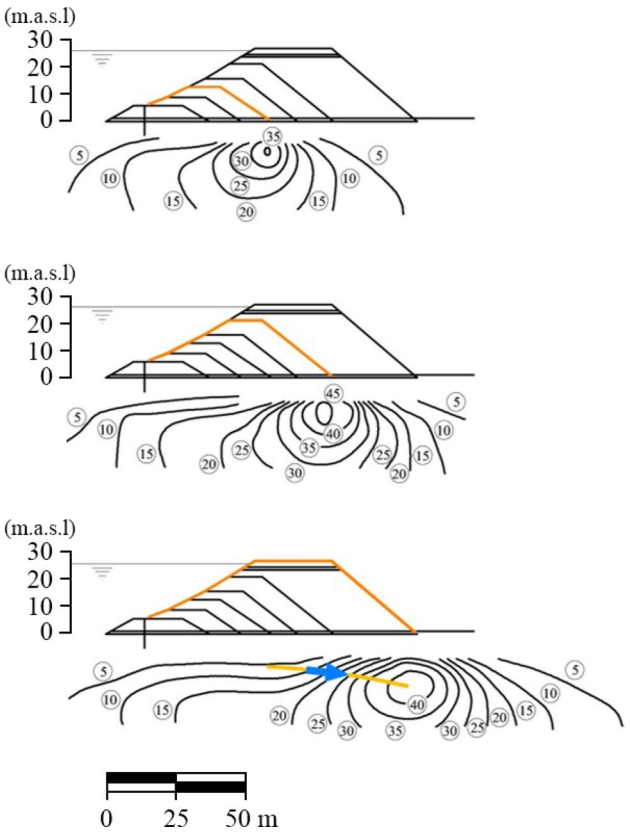

Fig. 12 Mobilized stress ratio in the clay foundation during dam construction

Figure 12 shows the theoretical mobilized friction angles in the clay foundation at three instants of the pond and dam construction. The maximum mobilized friction values occur below the downstream toe of the dam. They are high enough to exceed the peak strength and to trigger progressive failure. An indication of the position and development of a failure surface is plotted by an arrow line in Fig. 12.

A more precise analysis of the Aznalcóllar failure requires proper consideration of the foundation clay's brittle behaviour. Zabala and Alonso (2011) described a procedure to analyse the progressive failure of the dyke by means of a material point method (MPM). Fern et al. (2019) provides a comprehensive description of MPM and its application to geotechnical analysis, especially in cases requiring a dynamic formulation and large displacements. The following expression accounted for the strain softening behaviour of the blue clay in a Mohr–Coulomb elasto-plastic representation:

$$\text{Effective cohesion}: c' = c'_{peak}\, e^{-\eta \varepsilon^{p}_{eq}} \tag{1}$$

$$\text{Effective friction}: \phi' = \phi'_{res} + (\phi'_{peak} - \phi'_{res}) e^{-\eta \varepsilon^{p}_{eq}} \tag{2}$$

where $\varepsilon^{p}_{eq} = (2/3 e^{p} : e^{p})^{1/2}$ is the "equivalent" plastic shear strain, e^{p} is the deviatoric plastic strain tensor, and η is a parameter to control the rate of decay of strength with accumulated plastic shear strain. A value $\eta = 100$ was selected in view of experimental results and the size of the computational mesh.

Figure 13 shows the calculated evolution of the shear band for four instants of the dam construction. The model indicates that the first confined shear band developed at an advanced state of construction, about 4 years before the final failure. The model faithfully reproduced the position of the failure surface and its planar geometry. Also, the results were sensitive to the initial state of stress. The best agreement with the observations occurred at an at-rest coefficient of $K_0 = 1$, which is consistent with a moderately overconsolidated clay.

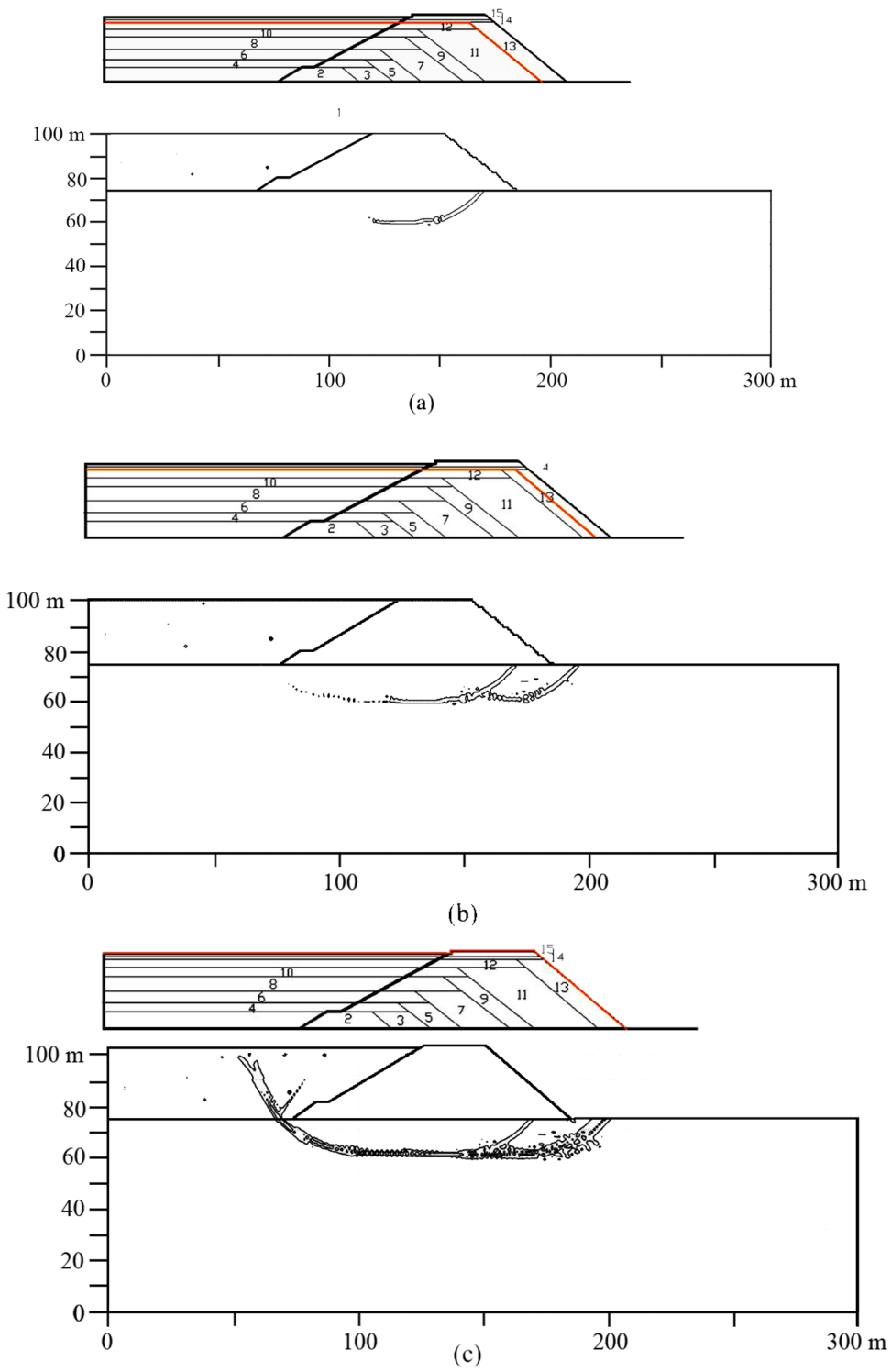

Fig. 13 **a–c** Development of the sliding surface for the final stages of dam construction. Plots indicate the contours of plastic deviatoric strain (1% and 5%). At rest coefficient: $K_0 = 1$

Dynamics

The tailings liquefied shortly after the forward motion of the dyke started, based on evidence that:

– The tailings flew out of the pond in a liquefied state and dispersed for 70 km of the Agrio and Guadiamar river valleys;

Fig. 14 Mud "volcanoes" observed a few hours after the failure on the surface of the depressed basin, upstream of the slid dam (Courtesy of J. M. Rodriguez Ortiz)

- Figure 14 is a photograph in the direction of the pond, taken from the crest of the displaced dyke. The presence of mud "volcanoes" everywhere is a clear indication of liquefaction;
- The distance travelled by the dyke (45–55 m) is difficult to explain without the propulsion provided by the liquefied tailings.

The third point was analysed in more detail. Figure 15 is a "free body" diagram of the slide. The stiff rockfill dyke move forward as a solid body without apparent distortion. A layer of clay and the alluvial terrace also moved forward sliding on a well-defined shearing surface which was, most likely, a sedimentation plane. This layer deformed in a passive manner at the toe of the slide.

On the opposite end, a large gap opened. This gap was bounded on the pond side by a subvertical "cliff", made possible by the already mentioned moderate cementation of tailings, but also by the undrained rapid unloading of the tailings. In fact, the low permeability of the tailings most likely resulted in negative excess pore water pressure, which helped stabilize the upstream scar opened in the tailings. The foot of this scar coincided with the upstream toe of the dyke slope. Therefore, the volume of tailings that liquefied initially occupied a wedge sitting on the upstream slope of the clay. A mantle of clay extended on the surface of the rockfill to prevent filtrations through the dam helped this wedge of tailings to fall into the open gap. The ensuing liquefaction was a result of the violent and intense deformation.

This description was used to draw Fig. 15 and to decide a procedure to estimate the dynamics of the motion. The idea was to accept that the motion could be analysed by a simple application of second Newton's law to the entire moving mass. If this was possible, the actual displacement (50 m) provides a benchmark to validate the model and find related dynamic variables (acceleration, velocity).

Since Aznalcóllar was a first-time failure in a brittle foundation, the initial instability implies an acceleration and the opening of an upstream gap. Subsequently, the fall of tailings into this gap and its liquefaction provided a pushing force, which was a function of the level of liquefied tailings upstream of the dyke. The "hydrostatic" pressure of tailings is high compared with water, because of the high unit weight of tailings (31 kN/m^3).

The constant volume of the unstable tailings wedge sitting above the upstream slope of the dam allowed the changing level of tailings during the motion to be calculated. The dynamic equilibrium of the moving body represented in Fig. 15, once the boundary forces are identified, leads to a simple dynamic equation for the velocity:

$$\frac{dv}{dt} = f(s(t),\ v(t)) \tag{3}$$

where $s(t)$ is the dyke displacement, shown in Fig. 15. Equation (3) is a nonlinear total differential equation solved by a finite difference scheme.

A static equilibrium analysis of the dam, foundation soils, and tailings at the time of failure (s = 0 in Fig. 15) is consistent with an average drained friction angle of 18° operating

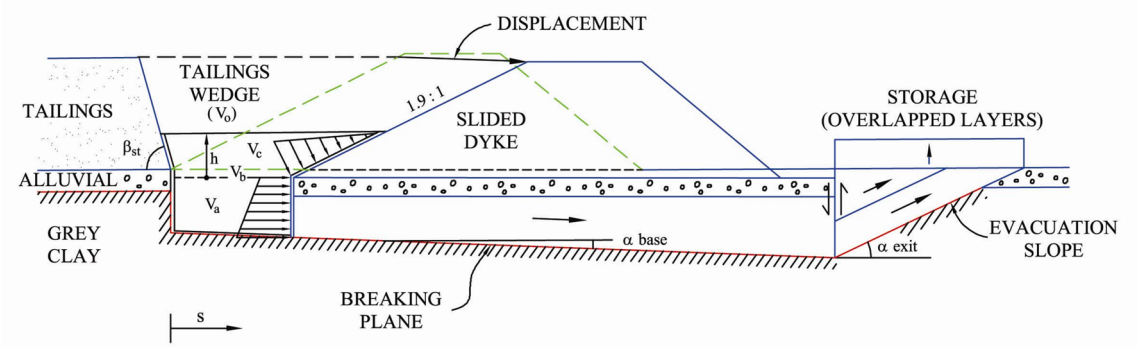

Fig. 15 Free body diagram of the forward motion of the dam and its foundation

on the sliding clay surface. As the dam accelerated and was displaced, the friction angle dropped to 11° along the entire failure surface (Alonso et al. 2010). Alonso and Gens (2006b) provides the details.

Figure 16 shows the calculated evolution of displacement, velocity, and acceleration of the dam. The calculated displacement matches the observations well. The passive wedge developing at the frontal part of the motion increased in resistance, but the main factor controlling the entire motion was the continuous reduction of tailings level pushing the dam. The calculated maximum velocity (Fig. 16) was slightly over 6 m/s (20 km/h) and the peak acceleration was 1.8 ms^{-2}. Overall, the estimated duration of the slide was 17 s.

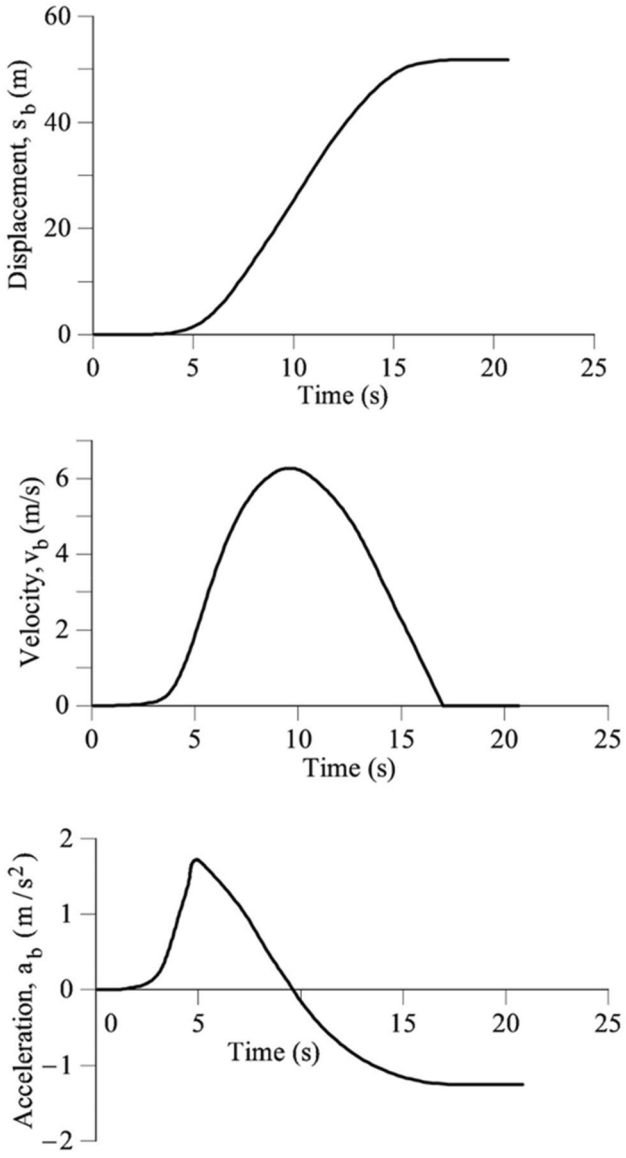

Fig. 16 The motion after failure: displacement, velocity, and acceleration records

More recently (Alonso 2020), an MPM analysis provided further insight and validation of the procedure outlined, using a strain-softening Mohr–Coulomb model to represent the blue clay foundation. Figure 17a shows the development of internal shearing strains when the slide came to rest. This result may be compared with the pattern of sliding surfaces observed in situ (Fig. 17b).

The Role of Clay Sedimentation Planes to Explain the Failure

The dyke north of the failed section (shown in the upper part of Fig. 5) was very similar to the southern one, but not identical. The height of the northern dyke decreased slowly towards the north and the pond received for several years a coarser and lighter material (pyroclast tailings), which may explain a smaller pushing force against the dyke. In addition, a significant difference of the northern and southern dykes is the orientation of sedimentation planes with respect to the expected direction of the tailings pushing force. The angle between the two traces was 19°. However, the dip direction of sedimentation planes is constant in the area occupied by the tailings pond. This difference may explain why the northern dyke did not fail.

Consider this situation in Fig. 18. Figure 18a shows the moving dyke and accompanying material slab resting on the stratification plane which is, potentially, the failure surface. The plot shows the weight W and its two components: normal to the failure plane (W_n) and in the direction of maximum slope (dip direction of clay strata; W_s). If the tailings thrust is perpendicular to the direction of the dykes, the figure also shows the force vectors E_1 and E_2 of the south and north basins of the pond, respectively. Note that E_1, if compared with E_2, is closer to the dip direction of the clay strata. Figure 18b and c show, in the stratification plane, the thrust vectors, the weight component W_s, and their resultant, $\overline{R}$. The angle α defines the direction of the force vectors E_1 and E_2.

In a limiting situation, the force vectors in Fig. 18b and c should be in equilibrium with the friction force generated in the sliding plane. This friction is proportional to the effective normal weight (W_n') of the moving mass. The calculation of (W_n') requires information on the pore pressures acting on the sliding surface, which was known because of the previous analysis.

In terms of the moduli of the force vectors mentioned, the equilibrium (Alonso and Gens 2006a) reads:

$$F^2 + 2FW \sin\alpha_b \sin\alpha + W^2 \sin^2\alpha_b - W_n'^2 \tan^2\phi' = 0 \quad (4)$$

where "F" is either E_1 or E_2. Equation (4) is a second order algebraic equation for the intensity of the tailing force necessary to trigger the failure. This force depends on the angle

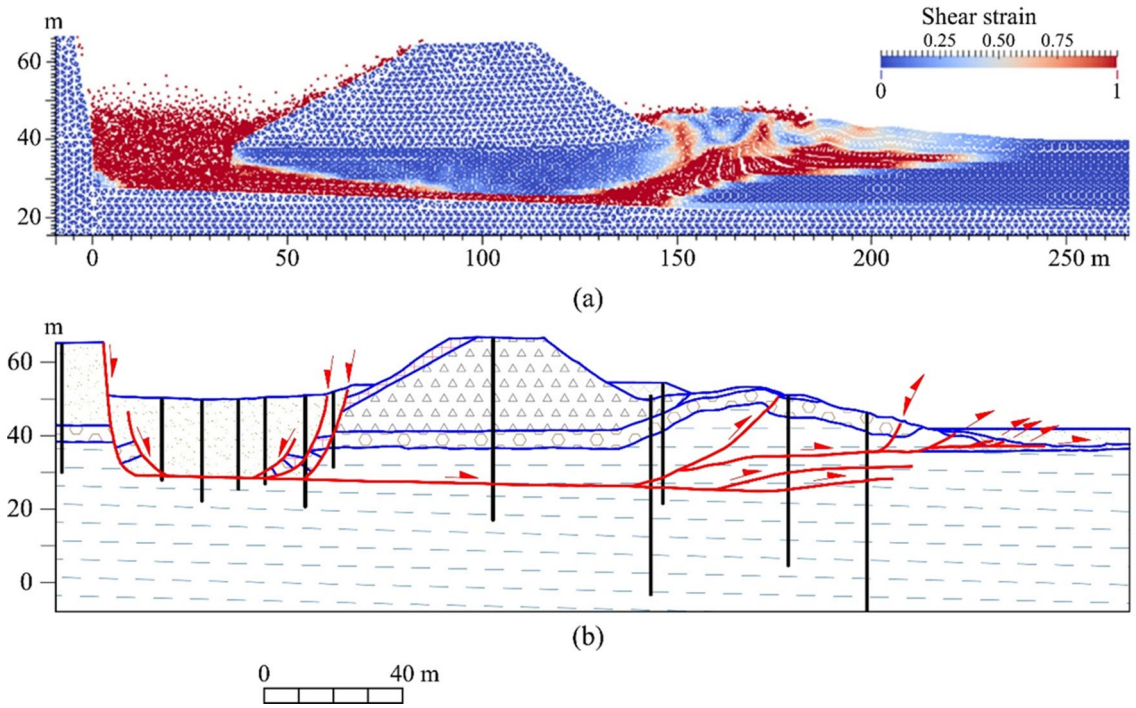

Fig. 17 **a** MPM analysis of Aznalcóllar failure. Shear strains contours. **b** Sliding surfaces identified "in situ"

α; α_b is the dip angle of the clay strata and has a low value (on average,$\alpha_b = 3°$).

Figure 19 shows the solution of Eq. (4). It provides the intensity of the force F in terms of the angle α in a polar diagram. The thrust against the southern dyke (the one that failed) has an angle $\alpha = 32°$ with respect to the horizontal direction of the sedimentation planes. The limiting force per unit length of the southern dyke is $E_1 = 420$ t/m (4.2 MN/m). A significantly higher force, $E_2 = 538$ t/m (5.38 MN/m) for $\alpha = 13°$ would have been required for the northern dyke to fail, because the tailings thrust of the northern basin "sees" the stratification planes with an effective dip angle close to 0.5°, while the southern dyke "sees" an inclination of the sliding plane of 2°. Figure 19 also shows the very significant change in the necessary force to trigger the instability when the pushing forces go against or in favour of a sliding surface dipping only 3°.

The polar plot in Fig. 19, which is a circle, is interpreted as the yielding surface in the two dimensional plane of forces F (for a given normal force W_n). In this plane, the direction normal to the circle represents the predicted direction of the displacement. The figure also shows this. The southern dyke rotated slightly towards the south during the motion. The preceding comment explains this field observation.

The Failure in Perspective

Our analysis of the failure indicated that the dyke construction sequence played a fundamental role in initiating a progressive failure mechanism, which eventually ended in a catastrophic failure. The effect of changing the construction procedure is an interesting issue, which has interest in practice (Alonso and Zabala 2012).

Conventional rockfill dams are built in layers in a manner that respects the planned position of the upstream and downstream slopes. A simplified procedure to represent this construction sequence in a numerical analysis is to apply, in a single step, the gravity loading to the final geometry of the dam. Another interesting way to check this is if a non-brittle soil exhibiting the average strength leading to failure, according to limit equilibrium ($c' = 0$, $\phi' = 18°$), would reproduce the observed failure under the actual staged construction. A further question in this regard is to investigate whether a different strain-softening mechanism (for instance, the friction angle remains constant while the effective cohesion drops to zero when shear strains accumulate) leads to the observed failure mechanism in Aznalcóllar. The last case may represent a bonded or cemented low plasticity clay. Table 1 describes

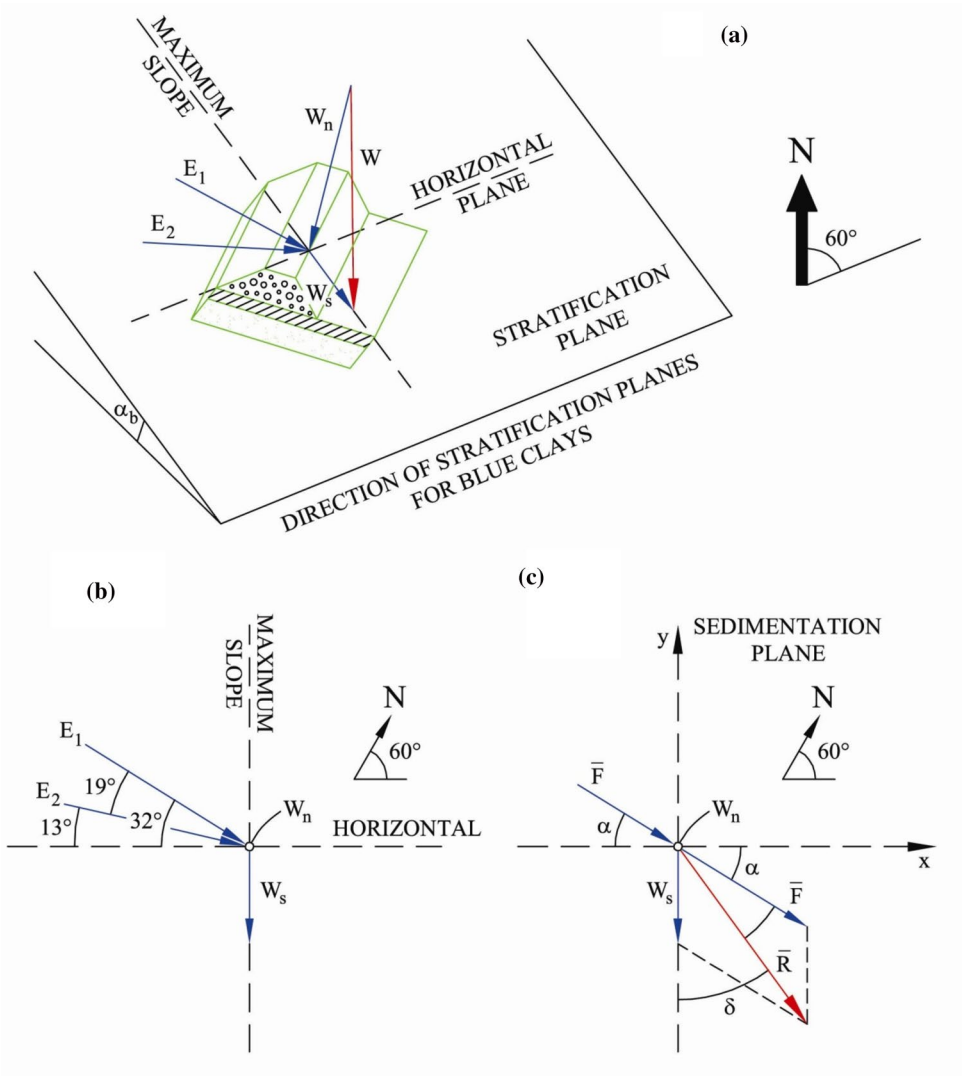

Fig. 18 **a** Scheme of a slice of the dam and its foundation soils sliding on a bedding plane; **b** forces acting on the slice; **c** resultant force

the cases outlined. Case 1 refers to the actual conditions of the Aznalcóllar failure. This case is the reference for the remaining three cases, 2, 3, and 4).

Case 2 leads to a perfectly stable situation despite the measured brittle behaviour of the Guadalquivir blue clay. Figure 20 shows the calculated contours of shearing deformation (0.1–1%) at the end of construction. The small confined shear band shown in the figure indicates stability.

Case 3 (Fig. 21) shows a fully developed failure surface, as expected, but its geometry is a "circle" failure, as also found in limit equilibrium in homogeneous soils. Case 4 (Figs. 22, 23) shows a tendency to develop a flattened rotational failure at an intermediate stage of construction, but at the final dyke height, the dominating shear band reproduces a circular failure.

It is concluded that the planar failure surface calculated in Case 1 (and observed in the field) resulted from both the downwards construction procedure and strain softening, which substantially reduced the effective cohesion and friction. To be more comprehensive, the development and geometry of the failure surface depends on:

- Details of the loading (and unloading) process leading to failure;
- The nature of strain softening;
- The pore water pressure evolution;
- The initial stress state.

Progressive failure phenomena are not commonly introduced in geotechnical design. If the objective is to determine a credible safety factor using standard procedures (limit equilibrium or (c',α') reduction methods in finite elements), finding rules to advance the average mobilized friction at failure has a practical interest. Figure 24 is an example. It shows the stress ratio (τ/σ'v) of a number of case histories compiled by Stark and Eid (1994). The three continuous lines provide the following information:

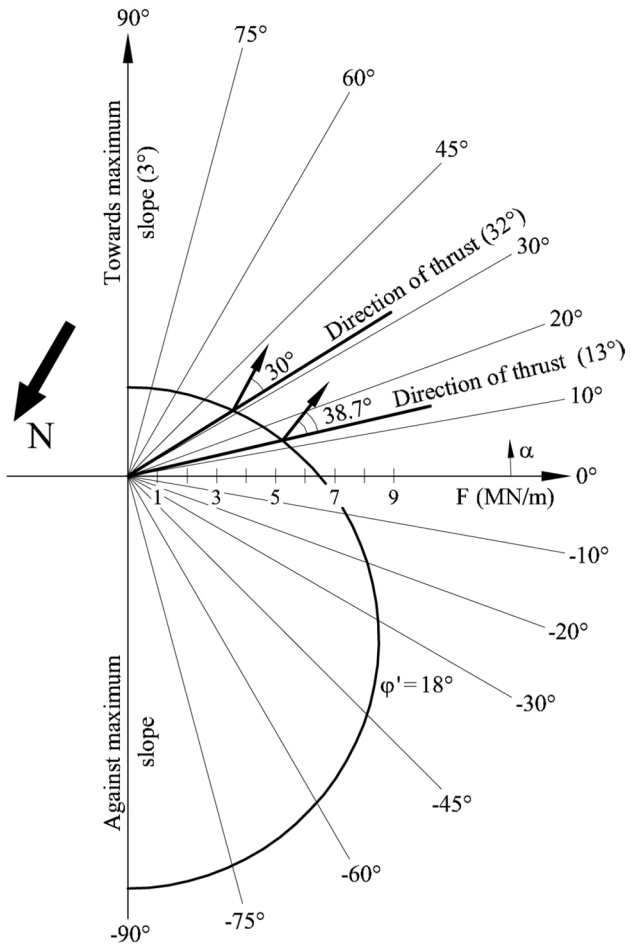

Fig. 19 Polar diagram showing the forces that induce dam sliding as a function of the direction of the thrust ($\alpha = 13°$ for the northern dyke; $\alpha = 32°$ for the southern dyke). The direction of motion (arrows normal to the force function) is also indicated

Table 1 Aznalcóllar dam failure. Sensitivity analysis ($K_0 = 1$). Cases analyzed

Case	Effective cohesion(*) [kPa]	Effective friction angle(*)	Construction sequence
1(+)	65→0	24°11°	Actual stage construction
2	65→0	24°11°	Single step. Weight applied progressively for 7300 days
3	0	17° (constant)	Actual staged construction
4	65→0	17° (constant)	Actual staged construction

(+) Base case. Actual conditions; (*) Mohr–Coulomb parameters of blue clay. The arrow indicates the assumed strain softening

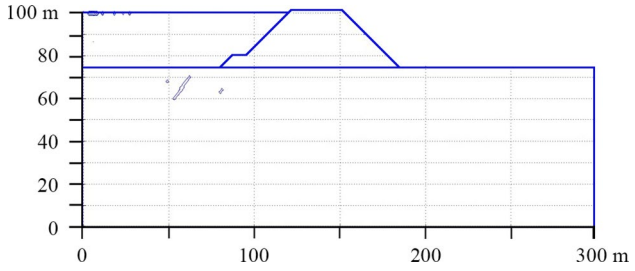

Fig. 20 Case 2. Dam built in a single step. Slow application (7300 days) of loading. Brittle blue clay cohesion drops from 64 kPa to 0. Friction drops from 24° to 11°. Contours of plastic shearing deformation of 0.1% and 1% at the end of construction

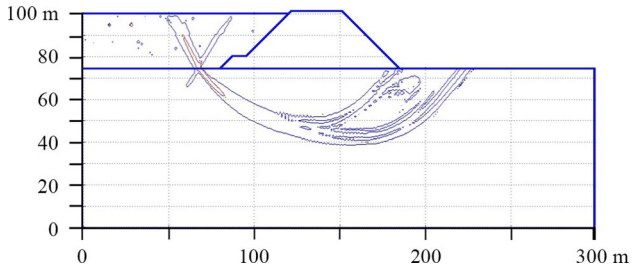

Fig. 21 Case 3. Actual staged construction. Constant strength parameters of blue clay: $c' = 0.\alpha' = 17°$. Contours of plastic shearing deformation of 1% and 5% at the end of construction

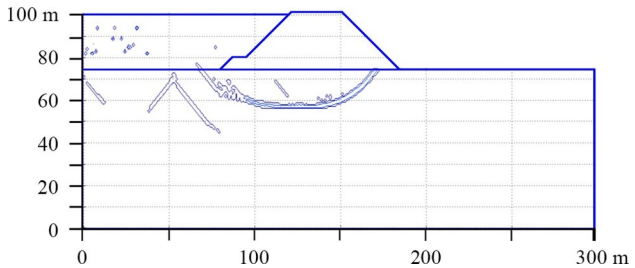

Fig. 22 Case 4. Actual staged construction. Strain softening of cohesion and constant friction: c´ drops from 64 kPa and $\alpha' = 17°$. Contours of plastic shearing deformation of 0.1% and 1% at an advanced stage of construction

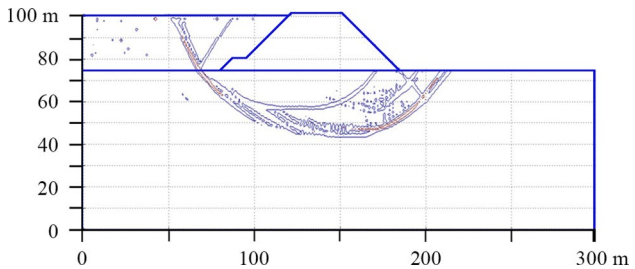

Fig. 23 Case 4. Actual staged construction. Strain softening of cohesion and constant friction: c´ drops from 64 kPa and $\alpha' = 17°$. Contours of plastic shearing deformation of 1% and 5% at the end of construction

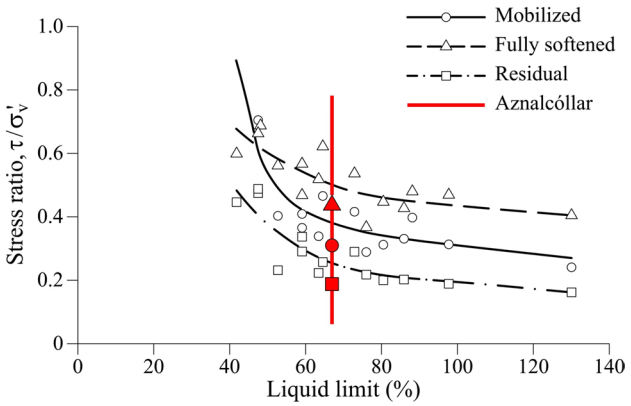

Fig. 24 Operating average stress ratio. Mobilized, fully softened and residual stress ratio from field case histories (Stark and Eid 1994). The Aznalcóllar case is also shown

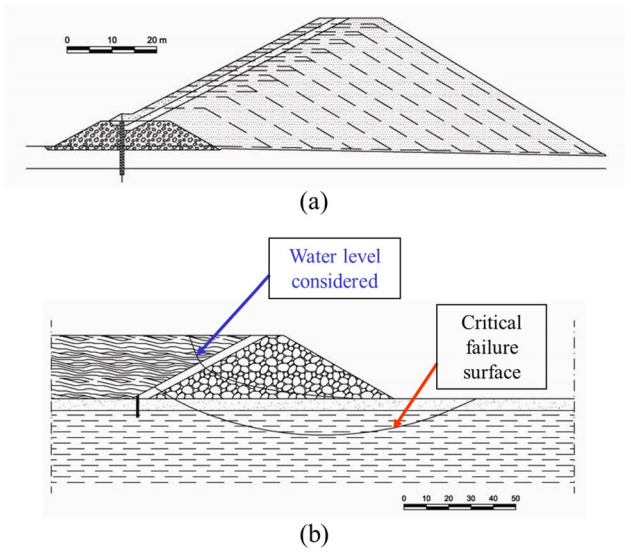

Fig. 25 Stability calculations during the design phase of the original project

– "Fully softened"—Equivalent to peak friction angle in absence of any effective cohesion;
– "Residual"—Determined in laboratory tests for large deformations;
– "Mobilized"—Determined by a back analysis of the actual field failure.

The friction ratios are shown to decrease with the plasticity of the clay involved in the failure. The figure shows that the mobilized strength for the Aznalcóllar case is at the mid-point between the peak and residual friction angles. A similar trend was found by Potts and Zdravkovic (2001) when analyzing slope failures in brittle clays. However, this is not a theoretical result and the averaged mobilized strength depends on all the aspects mentioned previously when discussing the geometry of the failure surface.

The Aznalcóllar dyke was designed in the 1970's. Figure 25a shows its cross-section geometry and illustrates the downward construction procedure. The dyke stability was analyzed under the following assumptions and loading actions:

– Tailings could liquefy;
– Pseudo-static vertical and horizontal accelerations $a_v = 0.776$ g; $a_h = 0.048$ g (for a design earthquake of magnitude MSK = 7);
– Water level given in Fig. 25b under stationary conditions;
– M-C strength parameters for the blue clay: c' = 0; f' = 20°.

The calculated safety factor in the original project, using the Morgenstern-Price method, was 1.3. Figure 25b shows the critical failure surface for the final height of the dam.

Despite the precautions adopted in some of the assumptions (liquefaction of tailings; earthquake loading) and the absence of any effective cohesion, the dyke failed. Figure 26

Fig. 26 Water pressures on the failure plane ("reference plane")

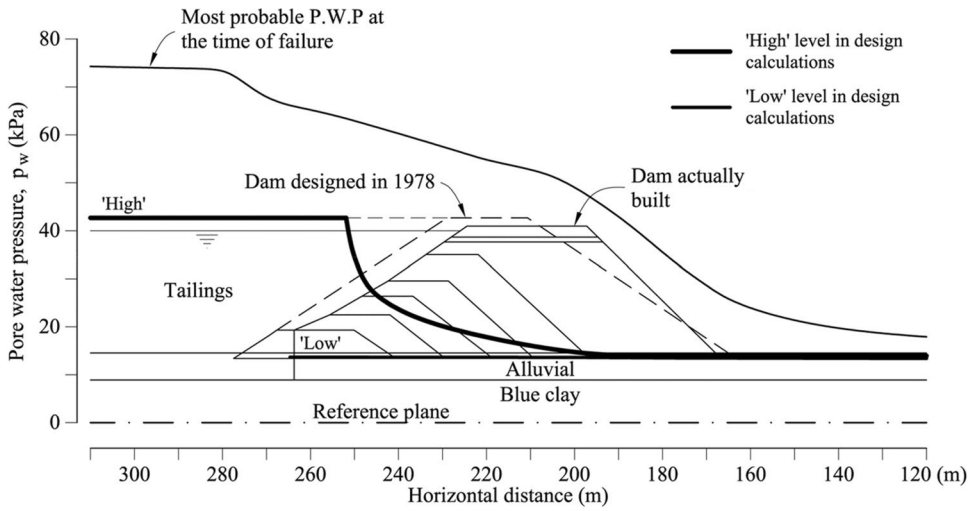

illustrates the reasons for the failure, which are summarized as follows:

- The most probable pore water pressure in the sliding surface ("reference plane" in the figure) at the time of failure was much larger than the pressures assumed in the original project. The figure shows the two alternatives assumed: either a "high" pressure or a "low" pressure, which was given by the free horizontal water level on the alluvial permeable layer. The "high" pressure profile was an interpretation of the condition of steady state percolation flow through the dam;
- The modification of the dyke profile during construction created a steeper slope at the downstream face of the dam. The steeper the slope, the higher the ratio of shear stress/effective normal stress on a sub-horizontal plane below the slope toe;
- No consideration of the progressive failure mechanism induced by the downstream dyke construction. In fact, the brittleness of the plastic blue clay was not recognized. The average friction selected (20°) is far higher than the residual friction (11°). However, the mentioned average operating friction on the failure surface (18°) does not differ much from the constant value assumed when designing the dyke.

Lessons Learned

A first general conclusion, even if more than 40 years have elapsed since the design of the dyke, is how difficult it is to interpret and quantify the behaviour of over-consolidated clay soils having: high plasticity, marked brittleness, low residual friction, low permeability, and a well-developed system of joints and discontinuities. It is also clear that downstream construction of retaining embankments enhances the risk of progressive failure.

A further general conclusion is that a standard hypothesis adopted to estimate pore water pressures in the dam and its foundation for the design of dams, namely the stationary flow condition, (Fell et al. 2005, Ch.11), goes against safety for low-permeability foundations soils. It is also recognized that the analysis must be drained; therefore, the relevant strength parameters are the effective cohesion and friction (c', ϕ'). c' is rather uncertain in most cases.

It has been shown that stability calculations not accounting for progressive failure should select an operational effective friction well below the peak friction angle and also controlled by residual friction (which decreases with increased plasticity). In addition, the pore water pressure, needed in the analysis, should be established by a consolidation transient analysis.

Potential failure mechanisms controlled by discontinuities should be explored. It has often been reported that the friction of joints is lower than the residual friction of the clay material.

Progressive failure is a common phenomenon but is difficult to analyse in practice. Field monitoring in these materials is difficult and there are only a few well documented case histories.

Finally, our analysis of the Aznalcóllar failure indicates that the geometry and position of the failure surface is a consequence of virtually all of the aspects controlling the development of progressive failure. Standard limit equilibrium analyses are poorly prepared to deal with the problem.

Acknowledgements The author wishes to thank Professors A. Gens (UPC), F. Zabala (U de San Juan) and A. Lloret (UPC) for their contributions to analysing the Aznalcóllar failure. Thanks are also extended to Dr. A. Yerro (Virginia Tech) and J. Moya (UPC). My deep appreciation also to the unknown peer reviewers of the paper and to the editorial team of the journal, Professor Rafael Fernández Rubio and Dr. Bob Kleinmann.

References

Alonso EE, Gens A (2006a) Aznalcóllar dam failure. Part 1: Field observations and material properties. Géotechnique 56(3):165–183

Alonso EE, Gens A (2006b) Aznalcóllar dam failure. Part 3: Dynamics of the motion. Géotechnique 56(3):203–210

Alonso EE, Pinyol NM, Puzrin A (2010) Geomechanics of failures. Springer, Dordrecht

Alonso EE, Zabala F (2012) Failure mechanisms in brittle soils: a dam failure revisited with the material point method. In: Khalili N, Oeser M (eds), Proc, Computer Methods for Geomechanics: Frontiers and New Applications, International Conf of the International Assoc for Computer Methods and Advances in Geomechanics, vol 1, pp 377–380

Alonso EE (2020) The motion and triggering of landslides. Géotechnique. https://doi.org/10.1680/jgeot.20.RL.001

Cooper MR, Bromhead EN, Petley DJ, Grant DI (1998) The Selborne cutting stability experiment. Géotechnique 48(1):83–101. https://doi.org/10.1680/geot.1998.48.1.83

Eriksson N, Adamek P (2000) The tailings pond failure of the Aznalcóllar Mine, Spain. In: Proc, 6th International Symp on Environmental Issues and Waste Management in Energy and Mineral Production. http://bc-mlard.ca/files/presentations/2016-19-ERIKSSON-ADAMEK-tailings-pond-failure-aznalcollar.pdf

Fell R, MacGregor P, Stapledon D, Bell G (2005) Geotechnical engineering of dams. Taylor & Francis Group, Balkema

Fern J, Rohe A, Soga K, Alonso EE (2019) The material point method for geotechnical engineering: a practical guide. CRC Press, Boca Raton

Gens A, Alonso EE (2006) Aznalcóllar dam failure. Part 2: Stability conditions and failure mechanism. Géotechnique 56(3):185–201. https://doi.org/10.1680/geot.2006.56.3.203

Potts DM, Dounias GT, Vaughan PR (1990) Finite element analysis of progressive failure of Carsington embankment. Géotechnique 40(1):79–101. https://doi.org/10.1680/geot.1990.40.1.79

Potts DM, Zdravkovic L (2001) Finite element analysis in geotechnical engineering: theory. Thomas Telford Ltd, London

Stark TD, Eid HT (1994) Slope stability analyses in stiff fissured clays. J Geotech Geoenviron 123(4):335–343

Yerro A, Pinyol NM, Alonso EE (2016) Internal progressive failure in deep-seated landslides. Rock Mech Rock Eng 49(6):1–16. https://doi.org/10.1007/s00603-015-0888-6

Zabala F, Alonso EE (2011) Progressive failure of Aznalcóllar dam using the material point method. Géotechnique 61(9):795–808